



New quantification of symmetry energy from neutron skin thicknesses of ^{48}Ca and ^{208}Pb

Rong An^{1,2} · Shuai Sun² · Li-Gang Cao^{2,3} · Feng-Shou Zhang^{2,3,4}

Received: 5 February 2024 / Revised: 16 June 2024 / Accepted: 21 June 2024 / Published online: 28 September 2024

© The Author(s), under exclusive licence to China Science Publishing & Media Ltd. (Science Press), Shanghai Institute of Applied Physics, the Chinese Academy of Sciences, Chinese Nuclear Society 2024

Abstract

Precise knowledge of the nuclear symmetry energy can be tentatively calibrated using multimessenger constraints. The neutron skin thickness of a heavy nucleus is one of the most sensitive indicators for probing the isovector components of effective interactions in asymmetric nuclear matter. Recent studies have suggested that the experimental data from the CREX and PREX2 collaborations are not mutually compatible with existing nuclear models. In this study, we review the quantification of the slope parameter of the symmetry energy L from the neutron skin thicknesses of ^{48}Ca and ^{208}Pb . Skyrme energy density functionals classified by various isoscalar incompressibility coefficients K were employed to evaluate the bulk properties of finite nuclei. The calculated results suggest that the slope parameter L deduced from ^{208}Pb is sensitive to the compression modulus of symmetric nuclear matter, but not that from ^{48}Ca . The effective parameter sets classified by $K = 220$ MeV can provide an almost overlapping range of L from ^{48}Ca and ^{208}Pb .

Keywords Nuclear symmetry energy · Neutron skin thickness · Energy density functional

This work was supported partly by the National Key R&D Program of China (No. 2023YFA1606401) and the National Natural Science Foundation of China (Nos. 12135004, 11635003, 11961141004, 12047513). L.-G. C. is grateful for the support of the National Natural Science Foundation of China (Nos. 12275025 and 11975096), and the Fundamental Research Funds for the Central Universities (No. 2020NTST06).

✉ Li-Gang Cao
caolg@bnu.edu.cn

✉ Feng-Shou Zhang
fszhang@bnu.edu.cn

¹ School of Physics, Ningxia University, Yinchuan 750021, China

² Key Laboratory of Beam Technology of the Ministry of Education, College of Nuclear Science and Technology, Beijing Normal University, Beijing 100875, China

³ Key Laboratory of Beam Technology of the Ministry of Education, Institute of Radiation Technology, Beijing Academy of Science and Technology, Beijing 100875, China

⁴ Center of Theoretical Nuclear Physics, National Laboratory of the Heavy Ion Accelerator of Lanzhou, Lanzhou 730000, China

1 Introduction

Nuclear symmetry energy (NSE), which characterizes the energy cost of converting isospin-symmetric nuclear matter (SNM) into pure neutron matter (PNM), plays a vital role in determining the properties of finite nuclei and neutron stars [1–5]. The density dependence of the NSE, that is, $E_{\text{sym}}(\rho)$, can be expanded around the saturation density ρ_0 ($\approx 0.16 \text{ fm}^{-3}$). The slope parameter L determines the behavior of the equation of state (EoS) for asymmetric nuclear matter in the vicinity of ρ_0 . Precise knowledge of the density dependence of the NSE is difficult to obtain owing to the uncertainties arising from the varying model-dependent slope parameter L . Fortunately, the characteristic behaviors of the NSE can be extracted indirectly from both extensive terrestrial nuclear experiments and observed astrophysical events [6–12].

Nuclear symmetry energy has been extensively used to encode the implications of the degree of isospin-asymmetry in finite nuclei. This is especially useful in the formation of the neutron skin thickness (NST) or neutron halo structures [13–15]. The quantity of NST, $\Delta R_{\text{np}} = \sqrt{\langle r_{\text{n}}^2 \rangle} - \sqrt{\langle r_{\text{p}}^2 \rangle}$, is defined as the difference between the root-mean-square (rms) radii of the neutrons and protons in a heavy nucleus

and is strongly correlated to the slope parameter of the NSE, L [16–35]. Therefore, the NST of a heavy nucleus was measured to provide a constraint on the EoS of neutron-rich matter around ρ_0 .

The neutron radius of ^{208}Pb has been determined in a laboratory by measuring the parity-violating asymmetry A_{PV} in polarized elastic electron scattering experiments such as PREX2 [36]. These efforts provided the latest value of NST with significantly improved precision: $\Delta R_{\text{np}}^{208} = 0.212\text{--}0.354$ fm. Moreover, a precise measurement of the NST for ^{48}Ca was updated by the CREX group: $\Delta R_{\text{np}}^{48} = 0.071\text{--}0.171$ fm [37]. The reported NST of ^{48}Ca is relatively thin compared to the measurement obtained by the high-resolution electric polarizability experiment (α_D) in the RCNP collaboration ($\Delta R_{\text{np}}^{48} = 0.14\text{--}0.20$ fm) [38]. In contrast, the NST of $\Delta R_{\text{np}}^{208}$ obtained by the PREX2 Collaboration is larger than that measured by RCNP ($\Delta R_{\text{np}}^{208} = 0.135\text{--}0.181$ fm) [39]. In Ref. [40], the NST of ^{208}Pb obtained by constraining astrophysical observables favors smaller values; for example, $\Delta R_{\text{np}}^{208} = 0.17 \pm 0.04$ fm. Likewise, the optimized new functionals obtained by calibrating the A_{PV} and α_D values of ^{208}Pb predict an NST of $\Delta R_{\text{np}}^{208} = 0.19 \pm 0.02$ fm and symmetry-energy slope of $L = 54 \pm 8$ MeV [41]. Recent theoretical studies have suggested that neutron star masses and radii are more sensitive to the NST of ^{208}Pb than its dipole polarizability α_D [42]. These results challenge our understanding of nuclear forces and energy density functionals (EDFs).

In Ref. [43], 207 EoSs were employed to explore the systematic correlations between $\Delta R_{\text{np}}^{48}$ and $L(\text{CREX})$ and between $\Delta R_{\text{np}}^{208}$ and $L(\text{PREX2})$. The slope parameter of the NSE obtained by fitting $\Delta R_{\text{np}}^{48}$ covers the interval range $L(\text{CREX}) = 0\text{--}50$ MeV; however, the calibrated correlation between the slope parameter L and $\Delta R_{\text{np}}^{208}$ yields $L(\text{PREX2}) = 76\text{--}165$ MeV. As mentioned in the literature, there is no overlap between $L(\text{CREX})$ and $L(\text{PREX2})$ at the one- σ level. A combined analysis was also performed using a recent experimental determination of the parity-violating asymmetry in ^{48}Ca and ^{208}Pb [44]. The study demonstrated that the existing nuclear EDFs cannot simultaneously offer an accurate description of the skins of ^{48}Ca and ^{208}Pb . The same scenario can also be encountered in Bayesian analyses, where the predicted $\Delta R_{\text{np}}^{48}$ is close to the CREX result, but considerably underestimates the result of $\Delta R_{\text{np}}^{208}$ with respect to the PREX2 measurement [45]. Considering the isoscalar–isovector couplings in relativistic EDFs, the constraints from various high-density data cannot reconcile the recent results from the PREX2 and CREX collaboration measurements [46]. These investigations indicate that it is difficult to provide consistent constraints for the isovector components of the EoSs using

existing nuclear EDFs, and further theoretical and experimental studies are urgently required [47].

To reduce the discrepancies between the different measurements and observations, an extra term controlling the dominant gradient correction to the local functional in the isoscalar sector has been used to weaken the correlations between the properties of the finite nuclei and the nuclear EoS [48]. As demonstrated in Ref. [49], the influence of the isoscalar sector is nonnegligible in the analysis. Nuclear matter properties expressed in terms of their isoscalar and isovector counterparts are correlated [50]. As noted above, existing discussions focus on the isovector components in the EDF models. Characteristic isoscalar quantities, such as the incompressibility of symmetric nuclear matter, are less considered when determining the slope parameter L [43]. The nuclear incompressibility can be deduced from measurements of the isoscalar giant monopole resonance (ISGMR) in medium-heavy nuclei [51, 52] and multi-fragmentations of heavy ion collisions [53]. The NSE obtained through the effective Skyrme-EDF is related to the isoscalar and isovector effective masses, which are also indirectly related to the incompressibility of symmetric nuclear matter [54]. Although correlations between the incompressibility coefficients and isovector parameters are generally weaker than correlations between the slope parameter L and NSE [55], quantification uncertainty due to nuclear matter incompressibility is inevitable in the evaluation. Therefore, the influence of the isoscalar nuclear matter properties is essential for evaluating slope parameter L .

The remainder of this paper is organized as follows. In Sect. 2, we briefly describe our theoretical model. In Sect. 3, we present the results and discussion. A short summary and outlook are provided in Sect. 4.

2 Theoretical framework

The sophisticated Skyrme-EDF, expressed as an effective zero-range force between nucleons with density- and momentum-dependent terms, has been succeeded in describing various physical phenomena [56–65]. In this study, Skyrme-like effective interactions were calculated as follows [66, 67]:

$$\begin{aligned} V(\mathbf{r}_1, \mathbf{r}_2) = & t_0(1 + x_0 \mathbf{P}_\sigma) \delta(\mathbf{r}) \\ & + \frac{1}{2} t_1(1 + x_1 \mathbf{P}_\sigma) [\mathbf{P}'^2 \delta(\mathbf{r}) + \delta(\mathbf{r}) \mathbf{P}^2] \\ & + t_2(1 + x_2 \mathbf{P}_\sigma) \mathbf{P}' \cdot \delta(\mathbf{r}) \mathbf{P} \\ & + \frac{1}{6} t_3(1 + x_3 \mathbf{P}_\sigma) [\rho(\mathbf{R})]^\alpha \delta(\mathbf{r}) \\ & + iW_0 \boldsymbol{\sigma} \cdot [\mathbf{P}' \times \delta(\mathbf{r}) \mathbf{P}], \end{aligned} \quad (1)$$

where $\mathbf{r} = \mathbf{r}_1 - \mathbf{r}_2$ and $\mathbf{R} = (\mathbf{r}_1 + \mathbf{r}_2)/2$ are related to the positions of two nucleons \mathbf{r}_1 and \mathbf{r}_2 , $\mathbf{P} = (\nabla_1 - \nabla_2)/2i$ is the

relative momentum operator and \mathbf{P}' is its complex conjugate acting on the left, and $\mathbf{P}_\sigma = (1 + \vec{\sigma}_1 \cdot \vec{\sigma}_2)/2$ is the spin exchange operator that controls the relative strength of the $S = 0$ and $S = 1$ channels for a given term in the two-body interactions, where $\vec{\sigma}_{1(2)}$ are Pauli matrices. The final term denotes the spin-orbit force, where $\sigma = \vec{\sigma}_1 + \vec{\sigma}_2$. Quantities α , t_i , and x_i ($i = 0-3$) represent the effective interaction parameters of the Skyrme forces.

Generally, effective interaction parameter sets are calibrated by matching the properties of finite nuclei and nuclear matter at the saturation density. Notably, the Skyrme-EDF can provide an analytical expression of all variables characterizing infinite nuclear matter (see [66–69] for details). The neutron skin of a heavy nucleus is regarded as a feasible indicator for probing isovector interactions in the EoS of asymmetric nuclear matter. Thus, the neutron and proton density distributions can be self-consistently calculated using Skyrme EDFs with various parameter sets. To clarify this, we further inspected the correlations between the slope parameter L and the NSTs of ^{48}Ca and ^{208}Pb . The bulk properties were calculated using standard Skyrme-type EDFs [51]. The corresponding effective interactions were in accord with the calculated nuclear matter properties, such as binding energy per nucleon $E = \mathcal{E}/\rho$, symmetry energy $E_{\text{sym}}(\rho) = \frac{1}{8}\partial^2(\mathcal{E}/\rho)/\partial\rho^2|_{\rho=\rho_0}$, slope parameter $L = 3\rho_0\partial E_{\text{sym}}(\rho)/\partial\rho|_{\rho=\rho_0}$, and the incompressibility coefficient $K = 9\rho_0^2\partial^2(\mathcal{E}/\rho)/\partial\rho^2|_{\rho=\rho_0}$. The value of the isoscalar incompressibility K from experimental data on giant monopole resonances covers a range of 230 ± 10 MeV [70, 71]. In addition, the incompressibility of symmetric nuclear matter deduced from α -decay properties is $K = 241.28$ MeV [72].

The nuclear breathing model exhibits a moderate correlation with the slope of the NSE and a strong dependence on the isoscalar incompressibility coefficient K of the symmetric nuclear matter [73]. The incompressibility of nuclear matter helps us understand the properties of neutron stars [74, 75]. Thus, it is essential to inspect the influence of isoscalar components on the slope parameter of the symmetry energy. To facilitate a quantitative discussion, a series of effective interaction sets classified by various nuclear incompressibility coefficients ($K = 220$ MeV, 230 MeV, and 240 MeV) were employed, as shown in Table 1. Generally, analytical expressions at the saturation density ρ_0 have specific forms [68]. Using these expressions, the density dependence of the symmetry energy can be expanded as a function of the neutron excess. Under the corresponding K , the slope parameter L and symmetry energy E_{sym} at the saturation density ρ_0 also cover a large range.

Table 1 Saturation properties with the different Skyrme parameter sets, such as symmetry energy E_{sym} (MeV), the slope parameter L (MeV) and the nuclear matter incompressibility coefficient K (MeV) at saturation density ρ_0 (fm^{-3}) [51, 68]

K (MeV)	Sets	E_{sym} (MeV)	L (MeV)
$K = 220$	s2028	28	5.21
	s2030	30	12.20
	s2032	32	33.31
	s2034	34	40.37
	s2036	36	58.82
	s2038	38	72.59
	s2040	40	83.22
	s3028	28	-11.23
	s3030	30	22.87
	s3032	32	36.22
$K = 230$	s3034	34	56.14
	s3036	36	71.54
	s3038	38	87.62
	s3040	40	106.09
	s4028	28	3.98
	s4030	30	34.07
	s4032	32	34.43
$K = 240$	s4034	34	62.59
	s4036	36	75.67
	s4038	38	98.65
	s4040	40	108.17

3 Results and discussions

In Fig. 1, the NSTs of ^{48}Ca and ^{208}Pb are determined under various effective interactions. The chosen parameter sets were classified by different incompressibility coefficients of symmetric nuclear matter, for example, $K = 220$ MeV, 230 MeV, and 240 MeV. The experimental constraint on the NST is indicated by a colored shadow. With increasing slope parameter L , the NST increases monotonically, and strong linear correlations between L and the NST of ^{48}Ca and ^{208}Pb are observed. As shown in Fig. 1(a), the linear correlations are similar, and the gradients for these three lines are in the range of $0.0008-0.0009$.

Figure 1(b) shows the related linear correlations between $\Delta R_{\text{np}}(^{208}\text{Pb})$ and the slope parameters L for various nuclear matter incompressibility coefficients. However, with increasing incompressibility coefficient, the slopes of the fitted lines gradually decrease or a large deviation emerges at a high L . The nuclear matter EoS is conventionally defined as the binding energy per nucleon and can be expressed as a Taylor series expansion in terms of the isospin asymmetry. As suggested in Ref. [73, 76], the compression modulus of symmetric nuclear matter is sensitive to the density dependence of the NSE. With increasing neutron star mass, the correlation

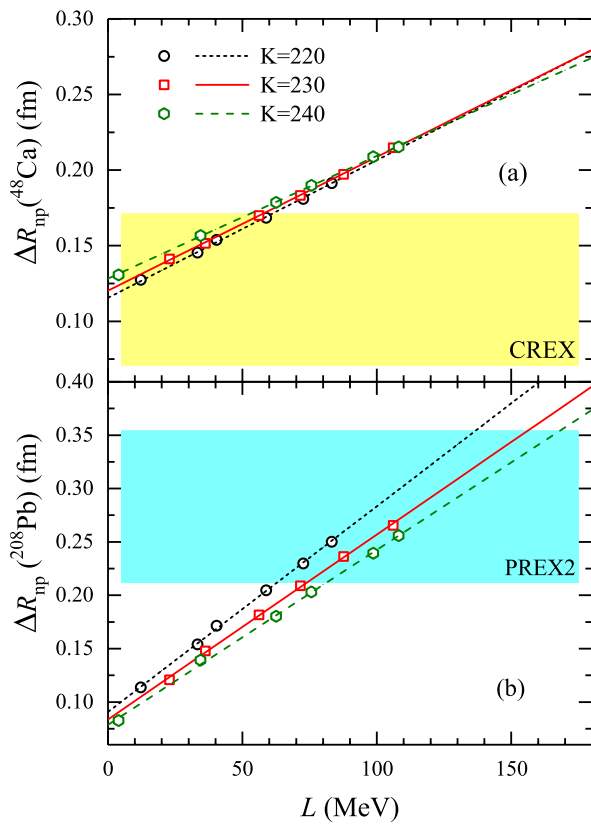


Fig. 1 (Color online) Neutron skin thickness of ^{48}Ca and ^{208}Pb as a function of slope parameter L at saturation density ρ_0 . Experimental constraints are indicated by horizontal light-yellow (a) and blue (b) bands. The open markers represent Skyrme-EDF calculations classified by various incompressibility coefficients. The corresponding lines indicate theoretical linear fits

between K and its slope L increases [75]. From this figure, we can see that the isoscalar quantity of the incompressibility coefficient has a significant influence on the determination of the slope parameter L for ^{208}Pb . However, for ^{48}Ca this influence can be ignored.

Herein, we assume that the value of L is positive. Linear functions were fitted to the data classified by various nuclear matter incompressibility coefficients using the least-squares method. For $K = 220$ MeV, we obtained the $L - \Delta R_{\text{np}}^{48}$ relationship as

$$\Delta R_{\text{np}}^{48} = 0.0009L + 0.1155 > 0.1155 \text{ fm.} \tag{2}$$

For $L - \Delta R_{\text{np}}^{208}$, the linear function $K = 220$ MeV is expressed as

$$\Delta R_{\text{np}}^{208} = 0.0019L + 0.0914 \text{ fm,} \tag{3}$$

where a high correlation coefficient is located at $R = 0.99$.

As suggested in Ref. [43], the slope parameter L (0–50 MeV) deduced from $\Delta R_{\text{np}}^{48}$ cannot overlap the interval

Table 2 Slope parameters L derived from the NSTs of ^{48}Ca and ^{208}Pb are shown by the classified isoscalar incompressibility coefficients

K (MeV)	$L - \Delta R_{\text{np}}^{48}$ (MeV)	$L - \Delta R_{\text{np}}^{208}$ (MeV)
220	0–60.96 (3.08)	62.94–136.65 (1.70)
230	0–57.64 (2.87)	74.05–155.99 (1.64)
240	0–52.78 (2.54)	81.35–168.01 (1.33)

The systematic uncertainties are presented in parenthesis

range of the slope parameter L (76–165 MeV) deduced from $\Delta R_{\text{np}}^{208}$. To facilitate a quantitative comparison of the experiments with these theoretical calculations, the slope parameters L derived from the constraints of the NSTs of ^{48}Ca and ^{208}Pb are presented for various nuclear matter incompressibility coefficients in Table 2. Remarkably, the gaps between $L - \Delta R_{\text{np}}^{48}$ and $L - \Delta R_{\text{np}}^{208}$ increase with increasing incompressibility coefficients from $K = 220$ MeV to 240 MeV.

Nuclear matter properties consisting of isovector and isoscalar components are correlated with each other. Ref. [50] suggests that there is no clear correlation between the incompressibility K and NSE, and between the slope of the NSE and incompressibility K . The correlations between K and the isovector parameters are generally weaker than those between the NST and NSE coefficients [18, 55]. As seen in Fig. 1(b), the increasing incompressibility coefficient K influences the determination of the covered range of the slope parameter L . Table 2 shows that the gap between $L - \Delta R_{\text{np}}^{48}$ and $L - \Delta R_{\text{np}}^{208}$ is smaller than the theoretical uncertainty when the nuclear incompressibility is $K = 220$ MeV. This is instructive for calibrating new sets of Skyrme parameters for reproducing various nuclear matter properties as auxiliary conditions.

To facilitate the influence of the incompressibility coefficient on determining the slope parameter L , the “data-to-data” relationships between the NST of ^{208}Pb and the incompressibility coefficients K are presented in Fig. 2. Here, the slope parameters of the NSE were chosen to be approximately $L = 34$ MeV and $L = 73$ MeV. From this figure, it can be seen that the NST of ^{208}Pb decreases with increasing incompressibility coefficient. This further demonstrates that the isoscalar compression modulus should be appropriately considered in the calibration protocol.

In our calculations, the upper limits of L were gradually overestimated as the incompressibility coefficient K increased. Combined with the latest PREX2 experiment, the result extracted from the relativistic EDFs leads to a covered range of $L = 106 \pm 37$ MeV [77]. The induced slope parameter L is more consistent with that obtained when the incompressibility coefficient is $K = 220$ MeV.

In Refs. [78–80], a highly linear correlation between the slope parameter L and the differences in the charge radii of

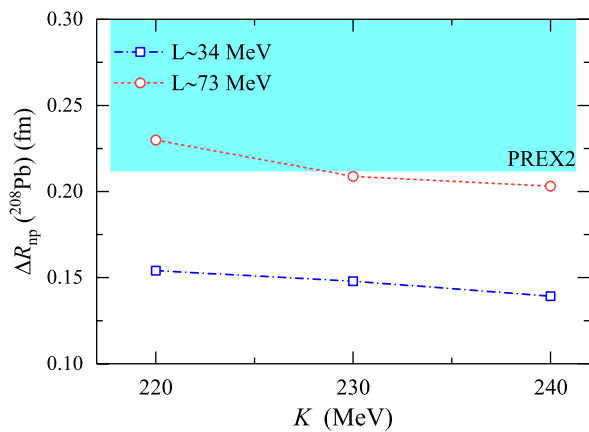


Fig. 2 (Color online) Neutron skin thickness of ^{208}Pb as a function of incompressibility coefficient K at saturation density ρ_0

mirror-partner nuclei ΔR_{ch} was demonstrated. The nuclear charge radius of ^{54}Ni has been determined using collinear laser spectroscopy [81]. By combining the charge radii of the mirror-pair nuclei ^{54}Fe , the deduced slope parameter covers the interval range $21 \text{ MeV} \leq L \leq 88 \text{ MeV}$. A recent study suggested that the upper or lower limits of L may be constrained if precise data on the mirror charge radii of ^{44}Cr – ^{44}Ca and ^{46}Fe – ^{46}Ca are selected [82]. In all of these studies, isoscalar nuclear matter properties were not considered. In fact, the value deduced from the relativistic and non-relativistic Skyrme EDFs with identical incompressibility coefficients $K = 230 \text{ MeV}$ gives a narrow range of $22.50 \text{ MeV} \leq L \leq 51.55 \text{ MeV}$ [83]. This is in agreement with the results in Ref. [84] where a soft EoS is obtained; for example, $L \leq 60 \text{ MeV}$.

In atomic nuclei, the NST is regarded as a perfect signal for describing the isovector property, and is highly correlated with the slope parameter of the NSE. The difference in the charge radii of the mirror-pair nuclei and the slope of the NSE exhibits a highly linear relationship [85–87]. To facilitate the influence of the isoscalar properties on determining the EoS of nuclear matter, the data-to-data relations between the difference in charge radii ΔR_{ch} of the mirror-pair nuclei ^{54}Ni – ^{54}Fe and the NSTs of ^{48}Ca and ^{208}Pb are shown in Fig. 3. Notably, highly linear correlations between ΔR_{ch} and the NSTs of ^{48}Ca and ^{208}Pb are observed.

In Fig. 3(a), the linear functions fit the experimental data well across various incompressibility coefficients K , that is, the slope parameter can be constrained concurrently through the calculated NST of ^{48}Ca and the ΔR_{ch} of mirror-pair nuclei ^{54}Ni – ^{54}Fe . However, as shown in Fig. 3(b), the fitting lines deviate from the cross-over region between ΔR_{ch} and the NST of ^{208}Pb except for $K = 220 \text{ MeV}$. Although the linear function captures a relatively narrow region, this further demonstrates the

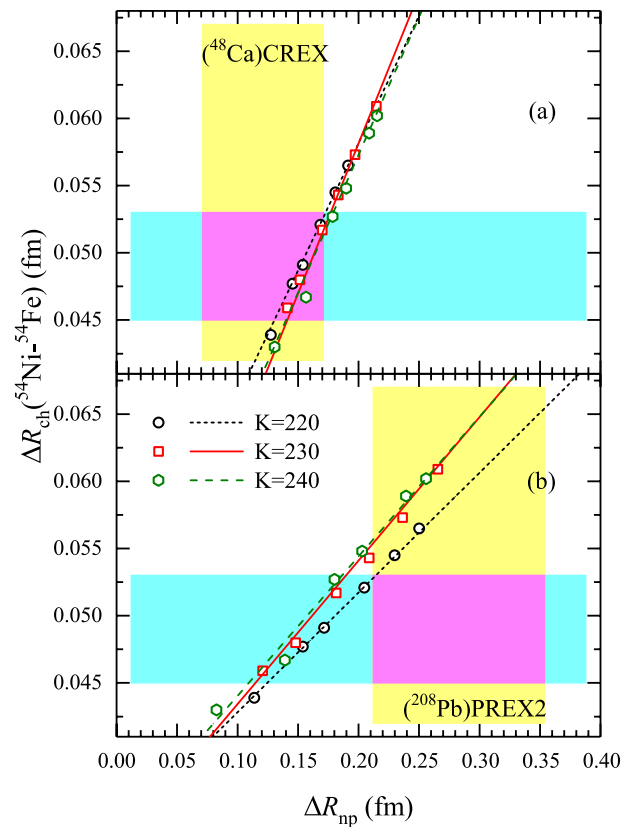


Fig. 3 (Color online) ΔR_{ch} of the mirror-pair nuclei ^{54}Ni – ^{54}Fe as a function of the neutron skin thicknesses of ^{48}Ca (a) and ^{208}Pb (b). The experimental constraints are shown as a horizontal light-blue band. The open markers are the results of Skyrme-EDF calculations. The corresponding lines indicate theoretical linear fits

need to extract valid information about the nuclear EoS by considering the isoscalar components in the calibration procedure.

The Coulomb term does not contribute to infinite nuclear matter calculations, in which the NSE plays an essential role in determining the evolution of isospin-asymmetry components. However, in atomic nuclei, the actual proton and neutron density distributions are mostly dominated by the degree of isospin asymmetry and Coulombic forces. It is evident that the competition between the Coulomb interaction and the NSE is related to the stability of the dripline nuclei against nucleon emission [88, 89]. The NST is associated with the symmetry energy and significantly influenced by the NSE, which corresponds to the EoS of neutron-rich matter. Meanwhile, a strong linear correlation between the slope parameter L and the difference in the charge radii of the mirror-pair nuclei is evident [78–83]. As shown in Fig. 3, this highly linear correlation extends to the NST and the difference in the

charge radii of the mirror-pair nuclei, owing to isospin-symmetry breaking [87].

4 Summary and outlook

As is well known, the Skyrme parameters can be characterized analytically by the isoscalar and isovector nuclear matter properties of the Hamiltonian density. More effective statistical methods have also been used to discuss the theoretical uncertainties [28, 90, 91]. In this study, we reviewed the influence of nuclear matter incompressibility on the determination of the slope parameter of the NSE L . The NSTs of ^{48}Ca and ^{208}Pb were calculated using Skyrme EDFs. The slope parameter L deduced from ^{208}Pb is sensitive to the incompressibility coefficients, whereas that for ^{48}Ca is not. A continuous range of L can be obtained if the nuclear matter is incompressible at $K = 220$ MeV. This is in agreement with that in Ref. [55] where the nuclear matter incompressibility covers the interval range of $K = 223_{-8}^{+7}$ MeV. This implies that isoscalar components should be considered when determining the slope parameter L . In addition, it is desirable to review the influence of the incompressibility coefficient K on the determination of the slope parameter L within the framework of relativistic EDFs.

The nuclear symmetry energy can be obtained using different methods and models [92–107]. The precise determination of the slope parameter L is related to various quantities such as the charge-changing cross-section [108, 109], sub-barrier fusion cross-section, and astrophysical S -factor in asymmetric nuclei [110]. Generally, the proton and neutron density distributions are mutually determined by the isospin asymmetry and Coulombic force. The isospin-symmetry-breaking effect influences the determination of the charge density distributions [111–114]. Thus, more accurate descriptions of NST and charge radii are required. In addition, the curvature of the symmetry energy K_{sym} [76] and three-body interactions in the Skyrme forces [115] may also influence the determination of the neutron skin.

Author Contributions All authors contributed to the study conception and design. Material preparation, data collection and analysis were performed by Rong An, Shuai Sun, Li-Gang Cao and Feng-Shou Zhang. The first draft of the manuscript was written by Rong An, and all authors commented on previous versions of the manuscript. All authors read and approved the final manuscript.

Declarations

Conflict of interest Feng-Shou Zhang is an editorial board member for Nuclear Science and Techniques and was not involved in the editorial review, or the decision to publish this article. All authors declare that there are no conflict of interest.

References

1. C.J. Horowitz, J. Piekarewicz, Neutron star structure and the neutron radius of ^{208}Pb . *Phys. Rev. Lett.* **86**, 5647 (2001). <https://doi.org/10.1103/PhysRevLett.86.5647>
2. B.-A. Li, P.G. Krastev, D.-H. Wen et al., Towards understanding astrophysical effects of nuclear symmetry energy. *Eur. Phys. J. A* **55**, 117 (2019). <https://doi.org/10.1140/epja/i2019-12780-8>
3. A.W. Steiner, M. Prakash, J.M. Lattimer et al., Isospin asymmetry in nuclei and neutron stars. *Phys. Rept.* **411**, 325 (2005). <https://doi.org/10.1016/j.physrep.2005.02.004>
4. J.M. Lattimer, M. Prakash, Neutron star observations: prognosis for equation of state constraints. *Phys. Rept.* **442**, 109 (2007). <https://doi.org/10.1016/j.physrep.2007.02.003>
5. J.F. Xu, C.J. Xia, Z.Y. Lu et al., Symmetry energy of strange quark matter and tidal deformability of strange quark stars. *Nucl. Sci. Tech.* **33**, 143 (2022). <https://doi.org/10.1007/s41365-022-01130-x>
6. B.-A. Li, L.-W. Chen, C.M. Ko, Recent progress and new challenges in isospin physics with heavy-ion reactions. *Phys. Rept.* **464**, 113 (2008). <https://doi.org/10.1016/j.physrep.2008.04.005>
7. B.-A. Li, A. Ramos, G. Verde et al., Topical issue on nuclear symmetry energy. *Eur. Phys. J. A* **50**, 9 (2014). <https://doi.org/10.1140/epja/i2014-14009-x>
8. J.-N. Hu, S.S. Bao, Y. Zhang et al., Effects of symmetry energy on the radius and tidal deformability of neutron stars in the relativistic mean-field model. *Prog. Theor. Exp. Phys.* **2020**, 043D01 (2020). <https://doi.org/10.1093/ptep/ptaa016>
9. Z. Zhang, L.-W. Chen, Constraining the density slope of nuclear symmetry energy at subsaturation densities using electric dipole polarizability in ^{208}Pb . *Phys. Rev. C* **90**, 064317 (2014). <https://doi.org/10.1103/PhysRevC.90.064317>
10. Y.-X. Zhang, M. Liu, C.-J. Xia et al., Constraints on the symmetry energy and its associated parameters from nuclei to neutron stars. *Phys. Rev. C* **101**, 034303 (2020). <https://doi.org/10.1103/PhysRevC.101.034303>
11. J. Liu, Z.-Z. Ren, C. Xu, Combining the modified Skyrme-like model and the local density approximation to determine the symmetry energy of nuclear matter. *J. Phys. G* **45**, 075103 (2018). <https://doi.org/10.1088/1361-6471/aac78f>
12. S. Yang, R.-J. Li, C. Xu, α clustering in nuclei and its impact on the nuclear symmetry energy. *Phys. Rev. C* **108**, L021303 (2023). <https://doi.org/10.1103/PhysRevC.108.L021303>
13. J. Meng, P. Ring, Relativistic Hartree–Bogoliubov description of the neutron halo in ^{11}Li . *Phys. Rev. Lett.* **77**, 3963 (1996). <https://doi.org/10.1103/PhysRevLett.77.3963>
14. S.-G. Zhou, J. Meng, P. Ring et al., Neutron halo in deformed nuclei. *Phys. Rev. C* **82**, 011301(R) (2010). <https://doi.org/10.1103/PhysRevC.82.011301>
15. X.-N. Cao, K.-M. Ding, M. Shi et al., Exploration of the exotic structure in Ce isotopes by the relativistic point-coupling model combined with complex momentum representation. *Phys. Rev. C* **102**, 044313 (2020). <https://doi.org/10.1103/PhysRevC.102.044313>
16. B.A. Brown, Neutron radii in nuclei and the neutron equation of state. *Phys. Rev. Lett.* **85**, 5296 (2000). <https://doi.org/10.1103/PhysRevLett.85.5296>
17. S. Typel, B.A. Brown, Neutron radii and the neutron equation of state in relativistic models. *Phys. Rev. C* **64**, 027302 (2001). <https://doi.org/10.1103/PhysRevC.64.027302>
18. S. Yoshida, H. Sagawa, Neutron skin thickness and equation of state in asymmetric nuclear matter. *Phys. Rev. C* **69**, 024318 (2004). <https://doi.org/10.1103/PhysRevC.69.024318>

19. L.-W. Chen, C.M. Ko, B.-A. Li, Nuclear matter symmetry energy and the neutron skin thickness of heavy nuclei. *Phys. Rev. C* **72**, 064309 (2005). <https://doi.org/10.1103/PhysRevC.72.064309>
20. X. Roca-Maza, M. Centelles, X. Viñas et al., Neutron skin of ^{208}Pb , nuclear symmetry energy, and the parity radius experiment. *Phys. Rev. Lett.* **106**, 252501 (2011). <https://doi.org/10.1103/PhysRevLett.106.252501>
21. M. Warda, X. Viñas, X. Roca-Maza et al., Neutron skin thickness in the droplet model with surface width dependence: indications of softness of the nuclear symmetry energy. *Phys. Rev. C* **80**, 024316 (2009). <https://doi.org/10.1103/PhysRevC.80.024316>
22. M.K. Gaidarov, A.N. Antonov, P. Sarriguren et al., Surface properties of neutron-rich exotic nuclei: a source for studying the nuclear symmetry energy. *Phys. Rev. C* **84**, 034316 (2011). <https://doi.org/10.1103/PhysRevC.84.034316>
23. M. Centelles, X. Roca-Maza, X. Viñas et al., Nuclear symmetry energy probed by neutron skin thickness of nuclei. *Phys. Rev. Lett.* **102**, 122502 (2009). <https://doi.org/10.1103/PhysRevLett.102.122502>
24. P.-G. Reinhard, W. Nazarewicz, Information content of a new observable: the case of the nuclear neutron skin. *Phys. Rev. C* **81**, 051303(R) (2010). <https://doi.org/10.1103/PhysRevC.81.051303>
25. B.K. Agrawal, J.N. De, S.K. Samaddar, Determining the density content of symmetry energy and neutron skin: an empirical approach. *Phys. Rev. Lett.* **109**, 262501 (2012). <https://doi.org/10.1103/PhysRevLett.109.262501>
26. B.K. Agrawal, J.N. De, S.K. Samaddar et al., Constraining the density dependence of the symmetry energy from nuclear masses. *Phys. Rev. C* **87**, 051306(R) (2013). <https://doi.org/10.1103/PhysRevC.87.051306>
27. N. Wang, L. Ou, M. Liu, Nuclear symmetry energy from the Fermi-energy difference in nuclei. *Phys. Rev. C* **87**, 034327 (2013). <https://doi.org/10.1103/PhysRevC.87.034327>
28. P.-G. Reinhard, W. Nazarewicz, Nuclear charge and neutron radii and nuclear matter: trend analysis in Skyrme density-functional-theory approach. *Phys. Rev. C* **93**, 051303(R) (2016). <https://doi.org/10.1103/PhysRevC.93.051303>
29. Z. Zhang, L.-W. Chen, Constraining the symmetry energy at sub-saturation densities using isotope binding energy difference and neutron skin thickness. *Phys. Lett. B* **726**, 234 (2013). <https://doi.org/10.1016/j.physletb.2013.08.002>
30. J. Xu, W.-J. Xie, B.-A. Li, Bayesian inference of nuclear symmetry energy from measured and imagined neutron skin thickness in $^{116,118,120,122,124,130,132}\text{Sn}$, ^{208}Pb , and ^{48}Ca . *Phys. Rev. C* **102**, 044316 (2020). <https://doi.org/10.1103/PhysRevC.102.044316>
31. J.M. Lattimer, Constraints on nuclear symmetry energy parameters. *Particles* **6**, 30 (2023). <https://doi.org/10.3390/particles6010003>
32. J.-M. Dong, W. Zuo, J.-Z. Gu, Constraints on neutron skin thickness in ^{208}Pb and density-dependent symmetry energy. *Phys. Rev. C* **91**, 034315 (2015). <https://doi.org/10.1103/PhysRevC.91.034315>
33. C. Xu, Z.-Z. Ren, J. Liu, Attempt to link the neutron skin thickness of ^{208}Pb with the symmetry energy through cluster radioactivity. *Phys. Rev. C* **90**, 064310 (2014). <https://doi.org/10.1103/PhysRevC.90.064310>
34. L.-W. Chen, C.M. Ko, B.-A. Li, Constraining the Skyrme effective interactions and the neutron skin thickness of nuclei using isospin diffusion data from heavy ion collisions. *Int. J. Mod. Phys. E* **15**, 1385–1395 (2006). <https://doi.org/10.1142/S0218301306004946>
35. J.-M. Dong, L.-J. Wang, W. Zuo et al., Constraints on Coulomb energy, neutron skin thickness in ^{208}Pb , and symmetry energy. *Phys. Rev. C* **97**, 034318 (2018). <https://doi.org/10.1103/PhysRevC.97.034318>
36. D. Adhikari, H. Albatineh, D. Androic et al., (PREX Collaboration), Accurate determination of the neutron skin thickness of ^{208}Pb through parity-violation in electron scattering. *Phys. Rev. Lett.* **126**, 172502 (2021). <https://doi.org/10.1103/PhysRevLett.126.172502>
37. D. Adhikari, H. Albatineh, D. Androic et al., (CREX Collaboration), Precision determination of the neutral weak form factor of ^{48}Ca . *Phys. Rev. Lett.* **129**, 042501 (2022). <https://doi.org/10.1103/PhysRevLett.129.042501>
38. J. Birkhan, M. Miorelli, S. Bacca et al., Electric dipole polarizability of ^{48}Ca and implications for the neutron skin. *Phys. Rev. Lett.* **118**, 252501 (2017). <https://doi.org/10.1103/PhysRevLett.118.252501>
39. A. Tamii, I. Poltoratska, P. von Neumann-Cosel et al., Complete electric dipole response and the neutron skin in ^{208}Pb . *Phys. Rev. Lett.* **107**, 062502 (2011). <https://doi.org/10.1103/PhysRevLett.107.062502>
40. R. Essick, I. Tews, P. Landry et al., Astrophysical constraints on the symmetry energy and the neutron skin of ^{208}Pb with minimal modeling assumptions. *Phys. Rev. Lett.* **127**, 192701 (2021). <https://doi.org/10.1103/PhysRevLett.127.192701>
41. P.-G. Reinhard, X. Roca-Maza, W. Nazarewicz, Information content of the parity-violating asymmetry in ^{208}Pb . *Phys. Rev. Lett.* **127**, 232501 (2021). <https://doi.org/10.1103/PhysRevLett.127.232501>
42. H. Sotani, T. Naito, Empirical neutron star mass formula based on experimental observables. *Phys. Rev. C* **107**, 035802 (2023). <https://doi.org/10.1103/PhysRevC.107.035802>
43. S. Tagami, T. Wakasa, M. Yahiro, Slope parameters determined from CREX and PREX2. *Res. Phys.* **43**, 106037 (2022). <https://doi.org/10.1016/j.rinp.2022.106037>
44. P.-G. Reinhard, X. Roca-Maza, W. Nazarewicz, Combined theoretical analysis of the parity-violating asymmetry for ^{48}Ca and ^{208}Pb . *Phys. Rev. Lett.* **129**, 232501 (2022). <https://doi.org/10.1103/PhysRevLett.129.232501>
45. Z. Zhang, L.-W. Chen, Bayesian inference of the symmetry energy and the neutron skin in ^{48}Ca and ^{208}Pb from CREX and PREX-2. *Phys. Rev. C* **108**, 024317 (2023). <https://doi.org/10.1103/PhysRevC.108.024317>
46. T. Miyatsu, M.-K. Cheoun, K. Kim et al., Can the PREX-2 and CREX results be understood by relativistic mean-field models with the astrophysical constraints? *Phys. Lett. B* **843**, 138013 (2023). <https://doi.org/10.1016/j.physletb.2023.138013>
47. E. Yüksel, N. Paar, Implications of parity-violating electron scattering experiments on ^{48}Ca (CREX) and ^{208}Pb (PREX-II) for nuclear energy density functionals. *Phys. Lett. B* **836**, 137622 (2023). <https://doi.org/10.1016/j.physletb.2022.137622>
48. C. Mondal, F. Gulminelli, Nucleonic metamodeling in light of multimessenger, PREX-II, and CREX data. *Phys. Rev. C* **107**, 015801 (2023). <https://doi.org/10.1103/PhysRevC.107.015801>
49. D. Chatterjee, F. Gulminelli, A.R. Raduta et al., Constraints on the nuclear equation of state from nuclear masses and radii in a Thomas-Fermi meta-modeling approach. *Phys. Rev. C* **96**, 065805 (2017). <https://doi.org/10.1103/PhysRevC.96.065805>
50. S. Yoshida, H. Sagawa, Isovector nuclear matter properties and neutron skin thickness. *Phys. Rev. C* **73**, 044320 (2006). <https://doi.org/10.1103/PhysRevC.73.044320>
51. G. Colò, N.V. Giai, J. Meyer et al., Microscopic determination of the nuclear incompressibility within the nonrelativistic framework. *Phys. Rev. C* **70**, 024307 (2004). <https://doi.org/10.1103/PhysRevC.70.024307>
52. L.-G. Cao, H. Sagawa, G. Colò, Microscopic study of the isoscalar giant monopole resonance in Cd, Sn, and Pb isotopes. *Phys. Rev. C* **86**, 054313 (2012). <https://doi.org/10.1103/PhysRevC.86.054313>

53. A. Ono, P. Danielewicz, W.A. Friedman et al., Symmetry energy for fragmentation in dynamical nuclear collisions. *Phys. Rev. C* **70**, 041604(R) (2004). <https://doi.org/10.1103/PhysRevC.70.041604>
54. L.-G. Cao, U. Lombardo, C.W. Shen et al., From Brueckner approach to Skyrme-type energy density functional. *Phys. Rev. C* **73**, 014313 (2006). <https://doi.org/10.1103/PhysRevC.73.014313>
55. J. Xu, Z. Zhang, B.-A. Li, Bayesian uncertainty quantification for nuclear matter incompressibility. *Phys. Rev. C* **104**, 054324 (2021). <https://doi.org/10.1103/PhysRevC.104.054324>
56. M. Bender, P.-H. Heenen, P.-G. Reinhard, Self-consistent mean-field models for nuclear structure. *Rev. Mod. Phys.* **75**, 121 (2003). <https://doi.org/10.1103/RevModPhys.75.121>
57. Y. Zhang, Y. Chen, J. Meng et al., Influence of pairing correlations on the radius of neutron-rich nuclei. *Phys. Rev. C* **95**, 014316 (2017). <https://doi.org/10.1103/PhysRevC.95.014316>
58. Y. Zhang, X.Y. Qu, Effects of pairing correlation on the quasi-particle resonance in neutron-rich Ca isotopes. *Phys. Rev. C* **102**, 054312 (2020). <https://doi.org/10.1103/PhysRevC.102.054312>
59. J.C. Pei, G.I. Fann, R.J. Harrison et al., Adaptive multi-resolution 3D Hartree–Fock–Bogoliubov solver for nuclear structure. *Phys. Rev. C* **90**, 024317 (2014). <https://doi.org/10.1103/PhysRevC.90.024317>
60. Q.Z. Chai, J.C. Pei, N. Fei et al., Constraints on the neutron drip line with the newly observed ^{39}Na . *Phys. Rev. C* **102**, 014312 (2020). <https://doi.org/10.1103/PhysRevC.102.014312>
61. Z.-J. Wu, L. Guo, Z. Liu et al., Production of proton-rich nuclei in the vicinity of ^{100}Sn via multinucleon transfer reactions. *Phys. Lett. B* **825**, 136886 (2022). <https://doi.org/10.1016/j.physletb.2022.136886>
62. L.-G. Cao, H. Sagawa, G. Colò, Effects of tensor correlations on low-lying collective states in finite nuclei. *Phys. Rev. C* **83**, 034324 (2011). <https://doi.org/10.1103/PhysRevC.83.034324>
63. P.-W. Wen, L.-G. Cao, J. Margueron et al., Spin-isospin response in finite nuclei from an extended Skyrme interaction. *Phys. Rev. C* **89**, 044311 (2014). <https://doi.org/10.1103/PhysRevC.89.044311>
64. E. Khan, N. Paar, D. Vretenar et al., Incompressibility of finite fermionic systems: stable and exotic atomic nuclei. *Phys. Rev. C* **87**, 064311 (2013). <https://doi.org/10.1103/PhysRevC.87.064311>
65. L.-G. Cao, S.-S. Zhang, H. Sagawa, Quenching factor of Gamow–Teller and spin dipole giant resonances. *Phys. Rev. C* **100**, 054324 (2019). <https://doi.org/10.1103/PhysRevC.100.054324>
66. E. Chabanat, P. Bonche, P. Haensel et al., A Skyrme parametrization from subnuclear to neutron star densities. *Nucl. Phys. A* **627**, 710 (1997). [https://doi.org/10.1016/S0375-9474\(97\)00596-4](https://doi.org/10.1016/S0375-9474(97)00596-4)
67. E. Chabanat, P. Bonche, P. Haensel et al., A Skyrme parametrization from subnuclear to neutron star densities Part II. Nuclei far from stabilities. *Nucl. Phys. A* **635**, 231 (1998). [https://doi.org/10.1016/S0375-9474\(98\)00180-8](https://doi.org/10.1016/S0375-9474(98)00180-8)
68. M. Dutra, O. Lourenço, J.S. Sá Martins et al., Skyrme interaction and nuclear matter constraints. *Phys. Rev. C* **85**, 035201 (2012). <https://doi.org/10.1103/PhysRevC.85.035201>
69. L.-W. Chen, C.M. Ko, B.-A. Li et al., Density slope of the nuclear symmetry energy from the neutron skin thickness of heavy nuclei. *Phys. Rev. C* **82**, 024321 (2010). <https://doi.org/10.1103/PhysRevC.82.024321>
70. D.H. Youngblood, H.L. Clark, Y.-W. Lui, Incompressibility of nuclear matter from the giant monopole resonance. *Phys. Rev. Lett.* **82**, 691 (1999). <https://doi.org/10.1103/PhysRevLett.82.691>
71. M. Uchida, H. Sakaguchi, M. Itoh et al., Systematics of the bimodal isoscalar giant dipole resonance. *Phys. Rev. C* **69**, 051301(R) (2004). <https://doi.org/10.1103/PhysRevC.69.051301>
72. W.M. Seif, α decay as a probe of nuclear incompressibility. *Phys. Rev. C* **74**, 034302 (2006). <https://doi.org/10.1103/PhysRevC.74.034302>
73. L.-W. Chen, J.-Z. Gu, Correlations between the nuclear breathing mode energy and properties of asymmetric nuclear matter. *J. Phys. G* **39**, 035104 (2012). <https://doi.org/10.1088/0954-3899/39/3/035104>
74. N. Alam, B.K. Agrawal, M. Fortin et al., Strong correlations of neutron star radii with the slopes of nuclear matter incompressibility and symmetry energy at saturation. *Phys. Rev. C* **94**, 052801(R) (2016). <https://doi.org/10.1103/PhysRevC.94.052801>
75. A. Kumar, H.C. Das, S.K. Patra, Incompressibility and symmetry energy of a neutron star. *Phys. Rev. C* **104**, 055804 (2021). <https://doi.org/10.1103/PhysRevC.104.055804>
76. J. Piekarewicz, Unmasking the nuclear matter equation of state. *Phys. Rev. C* **69**, 041301(R) (2004). <https://doi.org/10.1103/PhysRevC.69.041301>
77. B.T. Reed, F.J. Fattoyev, C.J. Horowitz et al., Implications of PREX-2 on the equation of state of neutron-rich matter. *Phys. Rev. Lett.* **126**, 172503 (2021). <https://doi.org/10.1103/PhysRevLett.126.172503>
78. N. Wang, T. Li, Shell and isospin effects in nuclear charge radii. *Phys. Rev. C* **88**, 011301(R) (2013). <https://doi.org/10.1103/PhysRevC.88.011301>
79. B.A. Brown, Mirror charge radii and the Neutron Equation of State. *Phys. Rev. Lett.* **119**, 122502 (2017). <https://doi.org/10.1103/PhysRevLett.119.122502>
80. B.A. Brown, K. Minamisono, J. Piekarewicz et al., Implications of the ^{36}Ca – ^{36}S and ^{38}Ca – ^{38}Ar difference in mirror charge radii on the neutron matter equation of state. *Phys. Rev. Res.* **2**, 022035(R) (2020). <https://doi.org/10.1103/PhysRevResearch.2.022035>
81. S.V. Pineda, K. König, D.M. Rossi et al., Charge radius of neutron-deficient ^{54}Ni and symmetry energy constraints using the difference in mirror pair charge radii. *Phys. Rev. Lett.* **127**, 182503 (2021). <https://doi.org/10.1103/PhysRevLett.127.182503>
82. Y.N. Huang, Z.Z. Li, Y.F. Niu, Correlation between the difference of charge radii in mirror nuclei and the slope parameter of the symmetry energy. *Phys. Rev. C* **107**, 034319 (2023). <https://doi.org/10.1103/PhysRevC.107.034319>
83. R. An, S. Sun, L.-G. Cao et al., Constraining nuclear symmetry energy with the charge radii of mirror-pair nuclei. *Nucl. Sci. Tech.* **34**, 119 (2023). <https://doi.org/10.1007/s41365-023-01269-1>
84. K. König, J.C. Berengut, A. Borschevsky et al., Nuclear charge radii of silicon isotopes. *Phys. Rev. Lett.* **132**, 162502 (2024). <https://doi.org/10.1103/PhysRevLett.132.162502>
85. J. Yang, J. Piekarewicz, Difference in proton radii of mirror nuclei as a possible surrogate for the neutron skin. *Phys. Rev. C* **97**, 014314 (2018). <https://doi.org/10.1103/PhysRevC.97.014314>
86. S.J. Novario, D. Lonardonì, S. Gandolfi et al., Trends of neutron skins and radii of mirror nuclei from first principles. *Phys. Rev. Lett.* **130**, 032501 (2023). <https://doi.org/10.1103/PhysRevLett.130.032501>
87. P. Bano, S.P. Pattnaik, M. Centelles et al., Correlations between charge radii differences of mirror nuclei and stellar observables. *Phys. Rev. C* **108**, 015802 (2023). <https://doi.org/10.1103/PhysRevC.108.015802>
88. X. Roca-Maza, N. Paar, Nuclear equation of state from ground and collective excited state properties of nuclei. *Prog. Part. Nucl. Phys.* **101**, 96 (2018). <https://doi.org/10.1016/j.pnpnp.2018.04.001>
89. K. Oyamatsu, K. Iida, H. Koura, Neutron drip line and the equation of state of nuclear matter. *Phys. Rev. C* **82**, 027301 (2010). <https://doi.org/10.1103/PhysRevC.82.027301>

90. L.E. Balliet, W.G. Newton, S. Cantu et al., Prior probability distributions of neutron star crust models. *Astrophys. J.* **918**, 79 (2021). <https://doi.org/10.3847/1538-4357/ac06a4>
91. P.-G. Reinhard, W. Nazarewicz, Information content of the differences in the charge radii of mirror nuclei. *Phys. Rev. C* **105**, L021301 (2022). <https://doi.org/10.1103/PhysRevC.105.L021301>
92. P. Giuliani, K. Godbey, E. Bonilla et al., Bayes goes fast: uncertainty quantification for a covariant energy density functional emulated by the reduced basis method. *Front. Phys.* **10**, 1054524 (2023). <https://doi.org/10.3389/fphy.2022.1054524>
93. R. Furnstahl, Neutron radii in mean-field models. *Nucl. Phys. A* **706**, 85 (2002). [https://doi.org/10.1016/S0375-9474\(02\)00867-9](https://doi.org/10.1016/S0375-9474(02)00867-9)
94. C. Mondal, B.K. Agrawal, M. Centelles et al., Model dependence of the neutron-skin thickness on the symmetry energy. *Phys. Rev. C* **93**, 064303 (2016). <https://doi.org/10.1103/PhysRevC.93.064303>
95. M. Gaidarov, I. Moumène, A. Antonov et al., Proton and neutron skins and symmetry energy of mirror nuclei. *Nucl. Phys. A* **1004**, 122061 (2020). <https://doi.org/10.1016/j.nuclphysa.2020.122061>
96. S.-H. Cheng, J. Wen, L.-G. Cao et al., Neutron skin thickness of ^{90}Zr and symmetry energy constrained by charge exchange spin-dipole excitations. *Chin. Phys. C* **47**, 024102 (2023). <https://doi.org/10.1088/1674-1137/aca38e>
97. L.-G. Cao, X. Roca-Maza, G. Colò et al., Constraints on the neutron skin and symmetry energy from the anti-analog giant dipole resonance in ^{208}Pb . *Phys. Rev. C* **92**, 034308 (2015). <https://doi.org/10.1103/PhysRevC.92.034308>
98. X. Roca-Maza, L.-G. Cao, G. Colò et al., Fully self-consistent study of charge-exchange resonances and the impact on the symmetry energy parameters. *Phys. Rev. C* **94**, 044313 (2016). <https://doi.org/10.1103/PhysRevC.94.044313>
99. L.-G. Cao, Z.-Y. Ma, Symmetry energy and isovector giant dipole resonance in finite nuclei. *Chin. Phys. Lett.* **25**, 1625 (2008). <https://doi.org/10.1088/0256-307x/25/5/028>
100. L.-G. Cao, Z.-Y. Ma, Soft dipole modes in neutron-rich Ni-isotopes in QRRPA. *Mod. Phys. Lett. A* **19**, 2845 (2004). <https://doi.org/10.1142/S0217732304015233>
101. M. Liu, Z.-X. Li, N. Wang et al., Exploring nuclear symmetry energy with isospin dependence on neutron skin thickness of nuclei. *Chin. Phys. C* **35**, 629 (2011). <https://doi.org/10.1088/1674-1137/35/7/006>
102. H. Yu, D.-Q. Fang, Y.-G. Ma, Investigation of the symmetry energy of nuclear matter using isospin-dependent quantum molecular dynamics. *Nucl. Sci. Tech.* **31**, 61 (2020). <https://doi.org/10.1007/s41365-020-00766-x>
103. S. Gautam, A. Venneti, S. Banik et al., Estimation of the slope of nuclear symmetry energy via charge radii of mirror nuclei. *Nucl. Phys. A* **1043**, 122832 (2024). <https://doi.org/10.1016/j.nuclphysa.2024.122832>
104. D.-Q. Fang, Neutron skin thickness and its effects in nuclear reactions. *Nucl. Tech. (in Chinese)* **46**, 080016 (2023). <https://doi.org/10.11889/j.0253-3219.2023.hjs.46.080016>
105. Z.-P. Gao, Q.-F. Li, Studies on several problems in nuclear physics by using machine learning. *Nucl. Tech. (in Chinese)* **46**, 080009 (2023). <https://doi.org/10.11889/j.0253-3219.2023.hjs.46.080009>
106. J. Xu, Constraining isovector nuclear interactions with giant dipole resonance and neutron skin in ^{208}Pb from a Bayesian approach. *Chin. Phys. Lett.* **38**, 042101 (2021). <https://doi.org/10.1088/0256-307X/38/4/042101>
107. W.-B. He, Q.-F. Li, Y.-G. Ma et al., Machine learning in nuclear physics at low and intermediate energies. *Sci. China Phys. Mech. Astron.* **66**, 282001 (2023). <https://doi.org/10.1007/s11433-023-2116-0>
108. J.-Y. Xu, Z.-Z. Li, B.-H. Sun et al., Constraining equation of state of nuclear matter by charge-changing cross section measurements of mirror nuclei. *Phys. Lett. B* **833**, 137333 (2022). <https://doi.org/10.1016/j.physletb.2022.137333>
109. J.-W. Zhao, B.-H. Sun, I. Tanihata et al., Isospin-dependence of the charge-changing cross-section shaped by the charged-particle evaporation process. *Phys. Lett. B* **847**, 138269 (2023). <https://doi.org/10.1016/j.physletb.2023.138269>
110. T. Ghosh, Sangeeta, G. Saxena et al., Neutron skin thickness dependence of astrophysical S-factor. *arXiv:2303.12156 [nucl-th]*, (2023). <https://doi.org/10.48550/arXiv.2303.12156>
111. J.-M. Dong, X.-L. Shang, W. Zuo et al., An effective Coulomb interaction in nuclear energy density functionals. *Nucl. Phys. A* **983**, 133 (2019). <https://doi.org/10.1016/j.nuclphysa.2019.01.003>
112. T. Naito, G. Colò, H.-Z. Liang et al., Toward *ab initio* charge symmetry breaking in nuclear energy density functionals. *Phys. Rev. C* **105**, L021304 (2022). <https://doi.org/10.1103/PhysRevC.105.L021304>
113. T. Naito, G. Colò, H.-Z. Liang et al., Effects of Coulomb and isospin symmetry breaking interactions on neutron-skin thickness. *Phys. Rev. C* **107**, 064302 (2023). <https://doi.org/10.1103/PhysRevC.107.064302>
114. C.-Y. Seng, M. Gorchtein, Electroweak nuclear radii constrain the isospin breaking correction to V_{ud} . *Phys. Lett. B* **838**, 137654 (2023). <https://doi.org/10.1016/j.physletb.2022.137654>
115. Z. Zhang, L.-W. Chen, Extended Skyrme interactions for nuclear matter, finite nuclei, and neutron stars. *Phys. Rev. C* **94**, 064326 (2016). <https://doi.org/10.1103/PhysRevC.94.064326>

Springer Nature or its licensor (e.g. a society or other partner) holds exclusive rights to this article under a publishing agreement with the author(s) or other rightsholder(s); author self-archiving of the accepted manuscript version of this article is solely governed by the terms of such publishing agreement and applicable law.